GEOPHYSICS, VOL. 85, NO. 4 (JULY-AUGUST 2020); P. A25–A29, 5 FIGS.
10.1190/GEO2019-0780.1

Migration with reduced artifacts from internal multiple reflections

Lele Zhang[1]

ABSTRACT

Migration of seismic reflection data leads to artifacts due to the presence of internal multiple reflections. Recent developments have shown that these artifacts can be avoided using Marchenko redatuming or Marchenko multiple elimination. These are powerful concepts, but their implementation comes at a considerable computational cost. We have derived a scheme to image the subsurface of the medium with significantly reduced computational cost and artifacts. This scheme is based on the projected Marchenko equations. The measured reflection response is required as input, and a data set with primary reflections and nonphysical primary reflections is created. Original and retrieved data sets are migrated, and the migration images are multiplied with each other, after which the square root is taken to give the artifact-reduced image. We showed the underlying theory and introduced the effectiveness of this scheme with a 2D numerical example.

INTRODUCTION

Standard migration schemes, including reverse time migration (RTM) and Kirchhoff migration, are based on the single-scattering assumption and are applied to measured reflection response to image the subsurface of the medium. The single-scattering assumption leads to artifacts when multiple reflections are present in the measured reflection response. These artifacts may cause erroneous interpretation. Several techniques have been proposed to deal with multiple reflections. Some techniques work in the data domain to remove multiple reflections, such that artifact-free subsurface image can be retrieved by standard migration schemes. Other techniques try to use the information embedded in multiple reflections to generate a better subsurface image.

Surface-related multiple elimination (SRME) (Verschuur et al., 1992) and inverse scattering series (ISS) (Weglein et al., 1997) are well-known schemes for attenuating multiple reflections in the data domain. The SRME scheme works to attenuate free-surface-related multiple reflections. The ISS scheme does not demand model information, but it tends to predict internal multiple reflections approximately (Weglein et al., 1997; Ten Kroode, 2002; Löer et al., 2016). Jakubowicz (1998) proposes to combine three primary reflections to predict and attenuate the first-order internal multiple reflections. Adaptive subtraction is required for the implementation of the schemes. Some researchers try to use multiple reflections in migration to improve the quality of the image (Reiter et al., 1991; Guitton, 2002; Ong et al., 2002). However, most of the schemes focus only on free-surface-related multiple reflections. Using internal multiple reflections in migration is done via full-wavefield migration (Berkhout, 2014), and a field data application is presented by Davydenko and Verschuur (2018).

Marchenko imaging is proposed to create artifact-free image of the subsurface (Slob et al., 2014; Wapenaar et al., 2014), and a variety of applications have been realized (da Costa Filho et al., 2014; Wapenaar and Slob, 2014; Singh et al., 2017; Ravasi, 2017; Zhang and Staring, 2018; Zhang et al., 2019). Van der Neut and Wapenaar (2016) propose a projected Marchenko scheme to avoid the estimation of the initial downgoing focusing function. Based on the projected version, Slob et al. (2017) derive an internal multiple elimination scheme, which retrieves primary and nonphysical primary reflections resulting from emitted events that eliminate internal multiple reflections. In this letter, we combine the measured reflection response and the retrieved data set to give an artifact-reduced migration scheme. The proposed scheme uses the same information as the conventional migration schemes but gives the artifact-reduced migration result at a significantly lower computational cost when compared with existing artifact-free migration schemes. Note that the proposed scheme is quite different from da Costa Filho and Curtis (2016) in the choice of the function used to combine two images and in its application to the coupled Marchenko equations. We start with the projected Marchenko equations and show how the data set containing primary and nonphysical primary reflections can be obtained. Then, we show how the artifact-

Manuscript received by the Editor 26 December 2019; revised manuscript received 22 February 2020; published ahead of production 18 March 2020; published online 7 May 2020.
[1]Delft University of Technology, 2628 CN Delft, The Netherlands. E-mail: l.zhang-1@tudelft.nl.

reduced subsurface image can be created from the measured and retrieved data set. A 2D complex numerical example is given to validate the performance, and we end with the discussions and conclusions.

THEORY

We indicate the reflection response as $R(\mathbf{x}_0', \mathbf{x}_0, t)$, where $\mathbf{x}_0$ is the source position, and $\mathbf{x}_0'$ is the receiver position, both placed at the boundary $\partial\mathbf{D}_0$, and t is the time. The reflection response $R(\mathbf{x}_0', \mathbf{x}_0, t)$ is assumed to be free of any free-surface effects. This means that, for the field data set, the free-surface-related multiple reflections and source and receiver ghosts need to be removed from the measured data set.

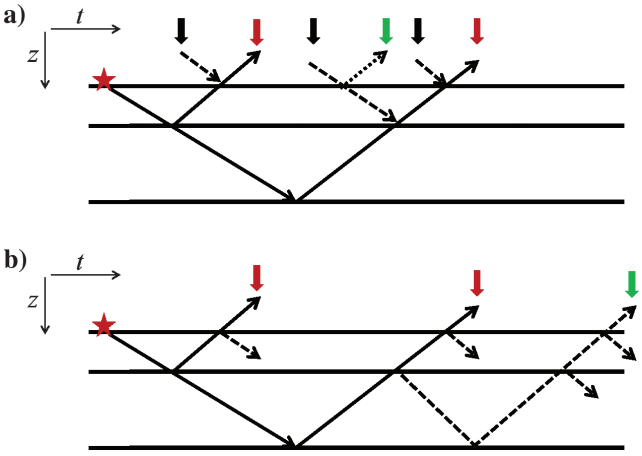

Figure 1. (a) One-dimensional sketch of the v^- in equations 1 and 2 with the focusing level at infinite depth. (b) One-dimensional sketch of the measured reflection response. In each plot, the red star indicates the source position, the red arrows indicate the primary reflections. The black arrows in (a) indicate the emitted events that eliminate internal multiple reflections. The green arrow in (a) indicates the nonphysical primary reflection resulting from the emitted event which eliminates the internal multiple reflection indicated by the green arrow in (b). The events indicated by green arrows in (a) and (b) have different travel time.

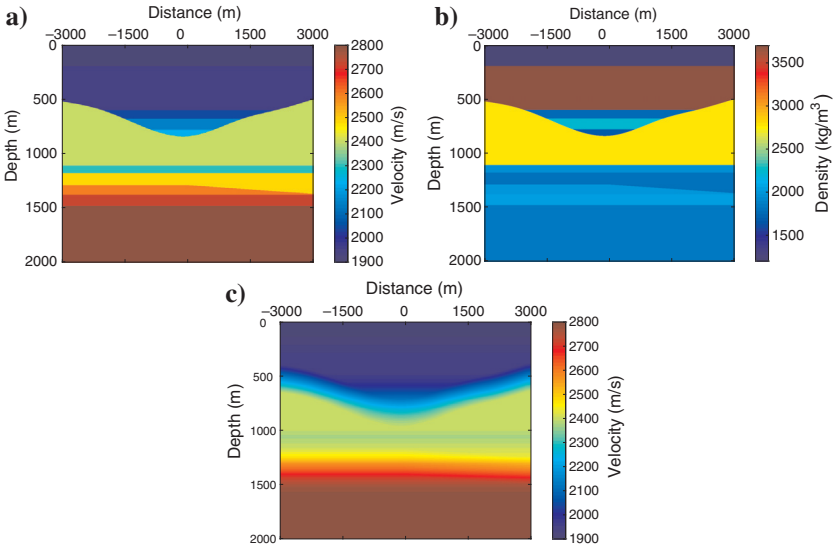

Figure 2. (a) Velocity and (b) density models, (c) the smoothed velocity model.

We follow van der Neut and Wapenaar (2016) to give the projected coupled Marchenko equations as

$$v^-(\mathbf{x}_0', \mathbf{x}_0'', t) = R(\mathbf{x}_0', \mathbf{x}_0'', t) + \int_{\partial\mathbf{D}_0} \mathrm{d}\mathbf{x}_0 \int_0^{+\infty} R(\mathbf{x}_0', \mathbf{x}_0, t') v^+(\mathbf{x}_0, \mathbf{x}_0'', t - t')\mathrm{d}t', \quad \text{for} \quad \varepsilon < t < t_2 - \varepsilon \qquad (1)$$

$$v^+(\mathbf{x}_0', \mathbf{x}_0'', t) = \int_{\partial\mathbf{D}_0} \mathrm{d}\mathbf{x}_0 \int_{-\infty}^0 R(\mathbf{x}_0', \mathbf{x}_0, -t') v^-(\mathbf{x}_0, \mathbf{x}_0'', t - t')\mathrm{d}t', \quad \text{for} \quad \varepsilon < t < t_2 - \varepsilon \qquad (2)$$

where $v^\pm$ indicates the projected down- and up-going focusing functions; the detailed definition can be found in van der Neut and Wapenaar (2016). Here, t_2 denotes a time value related to the subsurface focusing level, and ε is a small positive value which in practice can be taken as the half duration of the source signature. The projected coupled Marchenko equations can be solved iteratively for $v^\pm$ as

$$v_k^-(\mathbf{x}_0', \mathbf{x}_0'', t) = R(\mathbf{x}_0', \mathbf{x}_0'', t) + \int_{\partial\mathbf{D}_0} \mathrm{d}\mathbf{x}_0 \int_0^{+\infty} R(\mathbf{x}_0', \mathbf{x}_0, t') v_k^+(\mathbf{x}_0, \mathbf{x}_0'', t - t')\mathrm{d}t', \quad \text{for} \quad \varepsilon < t < t_2 - \varepsilon \qquad (3)$$

$$v_{k+1}^+(\mathbf{x}_0', \mathbf{x}_0'', t) = \int_{\partial\mathbf{D}_0} \mathrm{d}\mathbf{x}_0 \int_{-\infty}^0 R(\mathbf{x}_0', \mathbf{x}_0, -t') v_k^-(\mathbf{x}_0, \mathbf{x}_0'', t - t')\mathrm{d}t', \quad \text{for} \quad \varepsilon < t < t_2 - \varepsilon \qquad (4)$$

where $k = 0, 1, 2, \ldots$ indicates the iteration number, and the choice

$$v_0^+(\mathbf{x}_0', \mathbf{x}_0'', t) = 0, \qquad (5)$$

initializes the scheme given in equations 3 and 4. Thus, equations 1 and 2 can be iteratively solved for the projected focusing functions $v^\pm$ with the measured reflection response R as the only input.

As discussed by Slob et al. (2017), when the subsurface focusing level is chosen to be an infinite depth level (the t_2 in equations 1 and 2 is taken as an infinite positive value), the solved v^- consists of two parts: one part contains all primary reflections, which are also contained in measured reflection response; and another with the nonphysical primary reflections created after the processing. As shown in Figure 1, the created nonphysical primary reflections have different travel time from internal multiple reflections in the measured reflection response. However, the primary reflections in v^- have the same travel time with them in the measured reflection response, but higher amplitude because the transmission losses in primary reflections are compensated for after the processing. We use both data sets R and v^- to compute images with space-time image functions defined as

$$\mathbf{I}(\mathbf{x}_i,\mathbf{x}_i,t)=\int_{\partial\mathbf{D}_0}\mathrm{d}\mathbf{x}_0\int_{-\infty}^{+\infty}G_d^+(\mathbf{x}_i,\mathbf{x}_0,-t'')\times\int_{\partial\mathbf{D}_0}\mathrm{d}\mathbf{x}'_0\int_{-\infty}^{+\infty}v^-(\mathbf{x}'_0,\mathbf{x}_0,t-t'-t'')G_d^+(\mathbf{x}_i,\mathbf{x}'_0,-t')\mathrm{d}t'\mathrm{d}t'', \tag{6}$$

$$\mathbf{I}'(\mathbf{x}_i,\mathbf{x}_i,t)=\int_{\partial\mathbf{D}_0}\mathrm{d}\mathbf{x}_0\int_{-\infty}^{+\infty}G_d^+(\mathbf{x}_i,\mathbf{x}_0,-t'')\times\int_{\partial\mathbf{D}_0}\mathrm{d}\mathbf{x}'_0\mathbf{x}'_0\int_{-\infty}^{+\infty}R(\mathbf{x}'_0,\mathbf{x}_0,t-t'-t'')G_d^+(\mathbf{x}_i,\mathbf{x}'_0,-t')\mathrm{d}t'\mathrm{d}t'', \tag{7}$$

where $\mathbf{I}(\mathbf{x}_i,\mathbf{x}_i,t)$ and $\mathbf{I}'(\mathbf{x}_i,\mathbf{x}_i,t)$ are image functions, which can be used for estimating the image of the point $\mathbf{x}_i$ at $t=0$, G_d^+ is the wavefield extrapolation operator computed from a macro velocity model. The image estimated from $\mathbf{I}(\mathbf{x}_i,\mathbf{x}_i,t)$ contains artifacts arising from nonphysical primary reflections in v^- because these events are not real reflections from the subsurface; the image estimated from $\mathbf{I}'(\mathbf{x}_i,\mathbf{x}_i,t)$ contains artifacts arising from internal multiple reflections in R because these events are treated as primary reflections due to deeper reflectors. Generally, the internal multiple reflections in R and nonphysical primary reflections in v^- have different travel times, such that the artifacts present in both images are located in general at different places. However, the travel times of primary reflections are not changed after the processing, and they are migrated at same positions in both images. Thus, we combine both images retrieved from equations 6 and 7 to give a new image as

$$\bar{\mathbf{I}}(\mathbf{x}_i,\mathbf{x}_i,t)=\mathrm{sign}(\mathbf{I})\sqrt{\mathbf{I}(\mathbf{x}_i,\mathbf{x}_i,t)\mathbf{I}'(\mathbf{x}_i,\mathbf{x}_i,t)}. \tag{8}$$

where $\bar{\mathbf{I}}$ is the new image function. Artifacts in the image estimated from $\mathbf{I}$ are located in general at different places than artifacts in the image estimated from $\mathbf{I}'$, multiplying and taking square root presented in equation 8 can reduce the artifacts in the combined image. The image related to primary reflections is preserved during the processing.

EXAMPLE

The proposed scheme is validated using a 2D numerical example with velocity and density values shown in Figure 2a and 2b. The smoothed version of the velocity model is given in Figure 2c, which will be used to model the wavefield extrapolation operator G_d^+. The reflection responses have been modeled with 601 sources and 601 receivers at the upper boundary of the model. Because of the application of the absorbing boundary conditions, the modeled data sets are free of any free-surface effects. The source emits a Ricker wavelet with 20 Hz centre frequency. The modeled shot gather with source located at 0 m is shown in Figure 3a, in which the direct wave has been removed. We use the modeled data set as input to solve equations 3 and 4 iteratively for v^- with focusing level at the bottom of the model (putting the focusing level at an infinite depth is equivalent to putting the focusing level at the bottom of the model because v^- will be the same). The solved v^- with different iteration numbers $k=2$, $k=5$, $k=10$, and $k=20$ are given in Figure 3b–3e. In Figure 3b and 3c, the internal multiple reflections are partly suppressed, and nonphysical primary reflections are present. In Figure 3d and 3e, the internal multiple reflections are

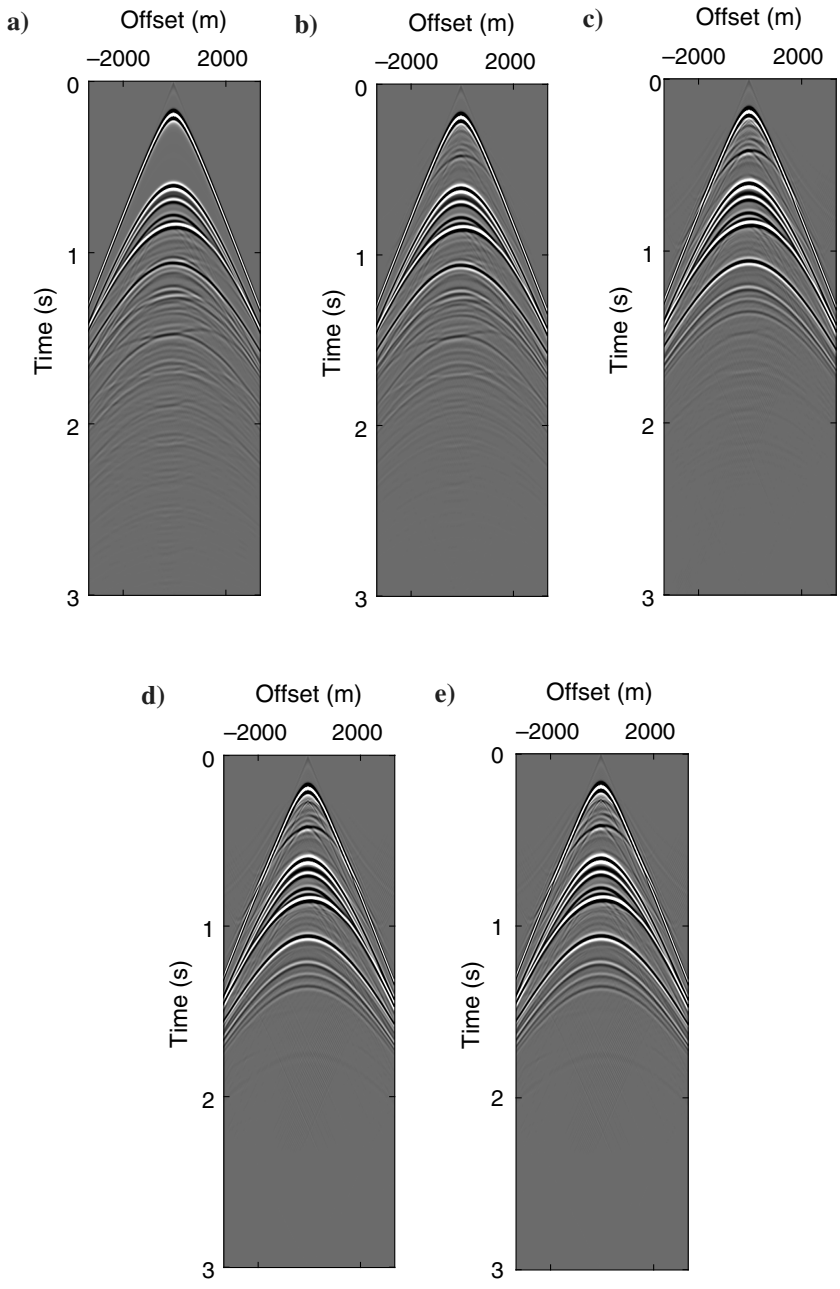

Figure 3. (a) The modeled reflection response. (b) The retrieved v^- with $k=2$, (c) the retrieved v^- with $k=5$, (d) the retrieved v^- with $k=10$, and (e) the retrieved v^- with $k=20$.

totally removed, and the energy of nonphysical primary reflections is stronger. Note that internal multiple reflections are mainly located at later arriving times as shown in Figure 3a, but the nonphysical primary reflections are mainly present at earlier arriving times as shown in Figure 3e. The zero-offset traces from the data sets shown in Figure 3a and 3e are picked and shown in Figure 4. The amplitude of primary reflections happens to be higher in v^- because the transmission losses have been compensated for after the processing. Also, nonphysical primary reflections have different travel time from internal multiple reflections in the modeled reflection response.

The modeled reflection responses and retrieved v^- are used as inputs to solve equations 6 and 7. The resulting images are given in Figure 5a and 5b. Note that artifacts due to internal multiple reflections (indicated by red arrows) mainly occur at deeper depth in Figure 5a, but the artifacts arising from nonphysical primary reflections (indicated by red arrows) are mainly present at shallower depth in Figure 5b. Then, the procedure as described in equation 8 leads to the image shown in Figure 5c. Artifacts present in Figure 5a and 5b are reduced in Figure 5c.

DISCUSSION

As explained in the theory section, the focusing level is positioned at infinite depth to derive the current scheme because in that case, the solved v^- contains all primary reflections from the subsurface. In the retrieved v^-, internal multiple reflections are removed, and nonphysical primary reflections are created as shown in Figure 3e. The presence of nonphysical primary reflections is a disadvantage. The modeled reflection responses and the retrieved data set are used for migration as described in equations 6 and 7. Finally, equation 8 leads to the resulting image with reduced artifacts. The current scheme is more time-consuming than regular RTM scheme, but the resulting image has fewer artifacts. The regular Marchenko imaging scheme which can be used to obtain image of subsurface without artifacts due to internal multiple reflections needs to solve the coupled Marchenko equations at every imaging point. It is much more expensive than the proposed scheme. The popular option of solving coupled Marchenko equations at a single-depth level and then performing local imaging (Wapenaar et al., 2014) is as cheap as the proposed scheme, but the artifacts arising from multiple reflections scattered in the target zone cannot be removed, which are significantly reduced by the proposed scheme. Besides, the proposed scheme also has the potential for improving regular multiple suppression procedures by using the original and multiple-attenuated data sets as inputs of equations 6 and 7 and retrieving artifact-reduced image from equation 8.

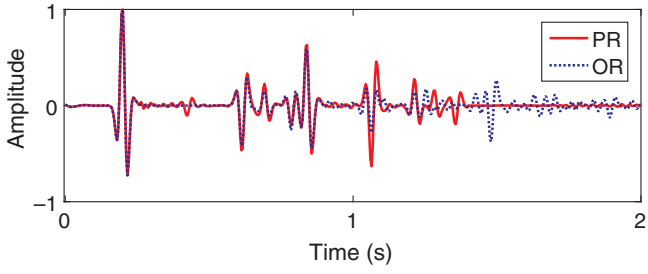

Figure 4. The comparison of zero-offset traces from modeled reflection response given in Figure 3a, and retrieved v^- given in Figure 3e. The red solid line (PR) indicates the zero-offset trace from the retrieved v^-, and the blue dotted line (OR) indicates the zero-offset trace from the modeled reflection response.

As shown in Figure 4, the primary reflections in the retrieved data set have higher amplitude than those in the modeled data set. That is why deeper reflectors in Figure 5b are stronger than those in Figure 5a. The procedure described in equation 8 balances the strengths of both images. It means that the image amplitudes obtained from equation 8 are not correct. The retrieved data set shown in Figure 3e indicates that, although nonphysical primary reflections occur everywhere, most of them are present at earlier times. Primary reflections from deeper reflectors in the retrieved data set are higher quality than those in the modeled data. Correspondingly, the deeper part of the image in Figure 5b is nearly artifact-free. Thus, the retrieved data set can be directly used to a nearly artifact-free image of the target zone of interest with focusing level positioned just below this zone. In that case, it can be seen as a target-driven migration scheme.

The green arrows in Figure 5a and 5b indicate artifacts arising from internal multiple reflections and nonphysical primary reflections. Both artifacts overlap by coincidence such that cannot be correctly dealt with by the proposed scheme. Correspondingly, they are not attenuated by equation 8 and still present in Figure 5c indicated by green arrow. Besides, from the migration images given in Figure 5a and 5b, we can see that the nonphysical primary reflections have different illumination aperture than the physical primary reflections, the detailed investigation on this topic is beyond the scope of this letter.

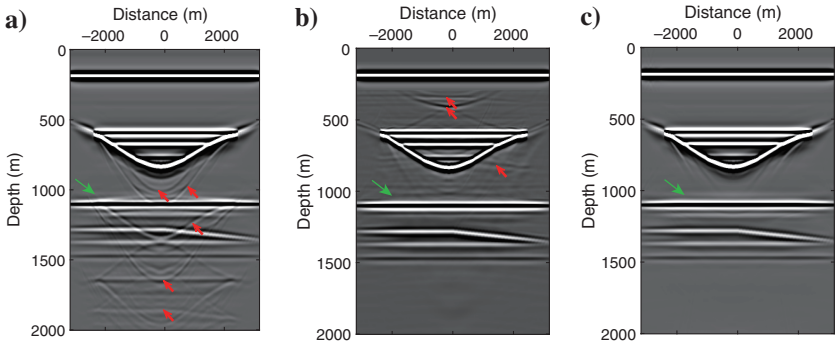

Figure 5. (a) Image of modeled reflection responses and (b) image of retrieved v^- with $k = 20$. (c) Artifact-reduced image retrieved by equation 8. Red arrows in (a) and (b) indicate artifacts arising from internal multiple reflections and nonphysical primary reflections.

CONCLUSION

We have shown that an artifact-reduced image can be constructed based on two data sets. One is the measured reflection response, and the other one is retrieved from the projected Marchenko equations by using the measured reflection response as input. The images obtained from both data sets contain artifacts located in general at different places and can be combined to generate an artifact-reduced subsurface image. The proposed migration scheme uses the same model information and measured reflection response as conventional migration schemes. The 2D numerical example shows that the scheme successfully images the subsurface of the medium with reduced artifacts.

ACKNOWLEDGMENTS

This work is part of the Open Technology Program with project number 13939, which is financed by NWO Domain Applied and Engineering Sciences. We would like to thank Evert Slob, Jeffrey Shragge, Joakim Blanch, Matteo Ravasi, and one anonymous reviewer for their valuable suggestions.

DATA AND MATERIALS AVAILABILITY

Data associated with this research are available and can be obtained by contacting the corresponding author.

REFERENCES

Berkhout, A. J., 2014, Review paper: An outlook on the future of seismic imaging — Part 2: Full-wavefield migration: Geophysical Prospecting, **62**, 931–949, doi: 10.1111/1365-2478.12154.

da Costa Filho, C. A., and A. Curtis, 2016, Attenuating multiple-related imaging artifacts using combined imaging conditions: Geophysics, **81**, no. 6, S469–S475, doi: 10.1190/geo2016-0113.1.

da Costa Filho, C. A., M. Ravasi, A. Curtis, and G. M. Meles, 2014, Elastodynamic Green's function retrieval through single-sided Marchenko inverse scattering: Physical Review E, **90**, 063201, doi: 10.1103/PhysRevE.90.063201.

Davydenko, M., and D. J. Verschuur, 2018, Including and using internal multiples in closed-loop imaging — Field data examples: Geophysics, **83**, no. 4, R297–R305, doi: 10.1190/geo2017-0533.1.

Guitton, A., 2002, Shot-profile migration of multiple reflections: 72nd Annual International Meeting, SEG, Expanded Abstracts, 1296–1299, doi: 10.1190/1.1816892.

Jakubowicz, H., 1998, Wave equation prediction and removal of interbed multiples: 68th Annual International Meeting, SEG, Expanded Abstracts, 1527–1530, doi: 10.1190/1.1820204.

Löer, K., A. Curtis, and G. A. Meles, 2016, Relating source-receiver interferometry to an inverse-scattering series to derive a new method to estimate internal multiples: Geophysics, **81**, no. 3, Q27–Q40, doi: 10.1190/geo2015-0330.1.

Ong, C., C. Lapilli, J. Perdomo, and R. Coates, 2002, Extended imaging and illumination in wave migrations: 72nd Annual International Meeting, SEG, Expanded Abstracts, 4116–4120, doi: 10.1190/segam2013-0614.1.

Ravasi, M., 2017, Rayleigh-Marchenko redatuming for target-oriented, true-amplitude imaging: Geophysics, **82**, no. 6, S439–S452, doi: 10.1190/geo2017-0262.1.

Reiter, E., M. Toksöz, T. Keho, and G. Purdy, 1991, Imaging with deepwater multiples: Geophysics, **56**, 1081–1086, doi: 10.1190/1.1443119.

Singh, S., R. Snieder, J. van der Neut, J. Thorbecke, E. Slob, and K. Wapenaar, 2017, Accounting for free-surface multiples in Marchenko imaging: Geophysics, **82**, no. 1, R19–R30, doi: 10.1190/geo2015-0646.1.

Slob, E., K. Wapenaar, F. Broggini, and R. Snieder, 2014, Seismic reflector imaging using internal multiples with Marchenko-type equations: Geophysics, **79**, no. 2, S63–S76, doi: 10.1190/geo2013-0095.1.

Slob, E., L. Zhang, and K. Wapenaar, 2017, Obtaining local reflectivity at two-way travel time by filtering acoustic reflection data: 87th Annual International Meeting, SEG, Expanded Abstracts, 4813–4817, doi: 10.1190/segam2017-17679411.1.

Ten Kroode, P. E., 2002, Prediction of internal multiples: Wave Motion, **35**, 315–338, doi: 10.1016/S0165-2125(01)00109-3.

van der Neut, J., and K. Wapenaar, 2016, Adaptive overburden elimination with the multidimensional Marchenko equation: Geophysics, **81**, no. 5, T265–T284, doi: 10.1190/geo2016-0024.1.

Verschuur, D., A. Berkhout, and K. Wapenaar, 1992, Adaptive surface-related multiple elimination: Geophysics, **57**, 1166–1177, doi: 10.1190/1.1443330.

Wapenaar, K., and E. Slob, 2014, On the Marchenko equation for multicomponent single-sided reflection data: Geophysical Journal International, **199**, 1367–1371, doi: 10.1093/gji/ggu313.

Wapenaar, K., J. Thorbecke, J. van der Neut, F. Broggini, E. Slob, and R. Snieder, 2014, Green's function retrieval from reflection data, in absence of a receiver at the virtual source position: Journal of the Acoustical Society of America, **135**, 2847–2861, doi: 10.1121/1.4869083.

Weglein, A. B., F. A. Gasparotto, P. M. Carvalho, and R. H. Stolt, 1997, An inverse scattering series method for attenuating multiples in seismic reflection data: Geophysics, **62**, 1975–1989, doi: 10.1190/1.1444298.

Zhang, L., and M. Staring, 2018, Marchenko scheme based internal multiple reflection elimination in acoustic wavefield: Journal of Applied Geophysics, **159**, 429–433, doi: 10.1016/j.jappgeo.2018.09.024.

Zhang, L., J. Thorbecke, K. Wapenaar, and E. Slob, 2019, Transmission compensated primary reflection retrieval in data domain and consequences for imaging: Geophysics, **84**, no. 4, Q27–Q36, doi: 10.1190/geo2018-0340.1.